Photoelectrochemical reactors for treatment of water and wastewater:

Emmanuel Mousset, Dionysios Dionysiou

Photo-Electrochemical Reactors for Treatment of Water and Wastewater

Emmanuel Mousset[1,*] and Dionysios D. Dionysiou[2,*]

[1] Laboratoire Réactions et Génie des Procédés, Université de Lorraine, CNRS, LRGP, F-54000 Nancy, France

[2] Environmental Engineering and Science Program, Department of Chemical and Environmental Engineering, 705 Engineering Research Center, University of Cincinnati, Cincinnati, OH 45221-0012, USA

REVIEW PAPER

ENVIRONMENTAL CHEMISTRY LETTERS

Corresponding authors:

E. Mousset (✉)

Laboratoire Réactions et Génie des Procédés, Université de Lorraine, CNRS, LRGP, F-54000 Nancy, France

email: emmanuel.mousset@univ-lorraine.fr

D.D. Dionysiou (✉)

Environmental Engineering and Science Program, Department of Chemical and Environmental Engineering, 705 Engineering Research Center, University of Cincinnati, Cincinnati, OH 45221-0012, USA

email: dionysios.d.dionysiou@uc.edu

Abstract

To address the increasing global water demand in parallel to water scarcity, especially exacerbated by the climate change, the "Water Reuse" option is more and more considered. It consists of the reuse of water for different sectors with different water quality requirement such as industry, agriculture and even for human consumption. The biotechnologies currently implemented are usually cheaper but are not sufficient to completely remove biorecalcitrant pollution. Advanced oxidation technologies for wastewater treatment have gained significant interests the last few years as an answer to this issue by producing very strong oxidizing agent such as hydroxyl radical (•OH) in mild conditions. Electrochemical advanced oxidation processes have attracted particular attention for water treatment through the continuous and *in situ* electro-catalytic generation of strong oxidizing species under mild conditions with the possibility to avoid the external addition of chemicals. The synergy between photochemical systems and electrolysis has more recently seen increasing interest considering benefits from using solar light as a free energy source. However, there is a lack of literature review on the reactions and engineering aspects of the photo-electrochemical reactors that play a paramount role on the overall process efficiency.

In this context, we reviewed the trends of photo-electrochemical reactors through two major points. Firstly, the reactions involved were presented along with the possible synergetic mechanisms. Under maximal conditions, eight •OH production sites could be identified when implementing photoelectro-Fenton combined with photoanodic oxidation and photocatalysis or photoelectrocatalysis. Several factors affect the occurrence of these reactions such as the solution pH, the applied wavelength, and the competition between reactions requiring the same reagent. Secondly, the different reactor design developed in response to the catalytic phenomena are discussed. Different configurations have been considered: sequential or hybrid reactors, divided or undivided cells, flow-cell or stirred tank reactor and light source positioning, i.e. external or immersed, vertical or horizontal, on the top or bottom or on the side of reactor. To obtain maximal synergy and maximum quantum yields, the distance between the light source and the electrode needs to be minimized. Hybrid reactors in undivided flow-cells are practically preferred for the lower footprint area, the possibility to regenerate iron catalysts and the enhancement of mass transfer compared with stirred tank reactor. Moreover, the interelectrode gap can be easily controlled in flow-cell, which permits optimisation of the

penetration depth when the light is applied through the reactor. These insights give some keys for future development of photo-electrochemical technologies.

Keywords Advanced oxidation • Anodic oxidation • Electrocatalysis • Electro-Fenton • Photocatalysis • Photo-electrochemical processes • Reactor design • Wastewater

Contents

1. Introduction

The release of hazardous micropollutants such as pesticides, pharmaceuticals and personal care products at the outlet of wastewater treatment plants into the water bodies is a problem of major concern (UNESCO 2017). These contaminants can be potentially toxic for the environment and human health even at very low concentrations (pg/L to µg/L) (Luo et al. 2014; Cizmas et al. 2015).

The biological processes involved in conventional treatment plants are not suitable enough to remove completely these biorecalcitrant compounds (Besnault and Martin 2011). Therefore, advanced physical-chemical technologies have been proposed to answer this issue and among them advanced oxidation processes have gained interest (Shi et al. 2020). They all rely on the generation of very strong oxidizing agents such as hydroxyl radicals (•OH) having a high standard potential ($E°$(•OH/H_2O)) that is equal to 2.80 V versus the standard hydrogen electrode, noted in V for the sake of simplicity in all the chapter (Glaze et al. 1987; Oturan and Aaron 2014; Stefan 2017). •OH radical is a reactive oxygen species that has a very short lifetime in the range of nanoseconds, which avoids its persistence into the environment (Gligorovski et al. 2015). •OH radical is also known for its almost non-selectivity due to its four reaction modes, i.e. hydrogen atom abstraction, electrophilic addition to unsaturated bonds, electron transfer and the ipso-substitution with perhalogenocarbon compounds, which permit the oxidation of a broad spectrum of compounds (Dorfman and Adams 1973; Von Sonntag 2008; Mousset et al. 2018a). •OH reaction is particularly fast with C=C double bonds that are present in molecular structure of many organic micropollutants, with oxidation rate constants ranging from 10^8 to 10^{10} L mol^{-1} s^{-1} (Mousset et al., 2016a).

Among advanced oxidation processes there are the traditional chemical ones that involve either (i) an oxidant such as hydrogen peroxide (H_2O_2) and a catalyst such as ferrous ion (Fe^{2+}), known as Fenton or Fenton-like processes, or (ii) photons produced by light irradiation photolysing an oxidant like H_2O_2 (Oturan and Aaron 2014). These processes present some drawbacks such as the need to continuously add reagents such as H_2O_2 (Oturan and Aaron 2014) or have applicability at a limited pH range. At the end of the nineties, the electrochemical-based advanced oxidation processes have been proposed as an alternative for producing *in situ* and continuously the oxidant species during the electrolysis, the electron being the main reagent involved (Brillas et al. 2009; Panizza and Cerisola 2009; Vasudevan and Oturan 2014; Sirés et al. 2014; Martínez-Huitle et al. 2015; Moreira et al. 2017). These characteristics make

electrochemical advanced oxidation processes gaining great interest in the scientific community since degradation and mineralisation yields can reached higher than 99% for a wide range of organic pollutant and organic load represented by a chemical oxygen demand below 100 g-O_2 L^{-1} (Lahkimi et al. 2007; Alcántara et al. 2009; Mousset et al. 2013, 2014a, b; Sirés et al. 2014; dos Santos et al. 2015, 2017; Shukla and Oturan 2015; Ganzenko et al. 2018).

More recently, photo-assisted electrochemical processes have been proposed in order to make use of renewable energy in response to the sustainable development objectives (Garcia-Segura et al. 2013; Garza-Campos et al. 2014; Ramirez et al. 2015; Mousset et al. 2017a). Photo-electrochemical processes have been applied for the treatment of biorefractory pollutants as reviewed recently (dos Santos and Scialdone 2018). Dyes are presents in textile effluents and they could be treated for discoloration and mineralisation (Martínez-Huitle and Brillas 2009; Zhao et al. 2010; Zhou et al. 2010; Xu et al. 2013; Brillas and Martínez-Huitle 2015). Pesticides released in wastewater (Fang et al. 2012; Almazán-Sánchez et al. 2017) have also been removed by photo-electrochemical processes. Pharmaceuticals detected as micropollutants in municipal wastewater treatment plants outflow or in hospital wastewaters could be degraded and mineralized (Zhao et al. 2009; Feng et al. 2013). Water disinfection is another promising application of such processes by inactivating pathogenic microorganisms such as bacteria like *Candida parapsilosis* and *Escherichia coli* (Liu et al. 2014; dos Santos and Scialdone 2018).

Interestingly, synergy in reactions can be obtained in photo-electrochemical combinations, especially in hybrid reactors. In fact, the reactor design represents an essential engineering aspects in photoprocesses efficiency. This is the reason why it is proposed to discuss those facets in the following sections.

2. Influence of catalytic oxidation

2.1. Selection of electrode materials for electrocatalytic oxidation

In electrochemical processes, electrode materials play a major role in the removal efficiency (Mousset et al., 2016c, 2016d; Mousset et al., 2017b; Oturan et al., 2012; Panizza and Martinez-Huitle, 2013; Yu et al., 2015; Zhou et al., 2014). According to their properties they will act as catalyst to promote or not the oxidation of organic and inorganic compounds. There are two ways of oxidation, either by direct electron exchange through redox reactions with electroactive species, i.e. the so-called direct oxidation, or the indirect oxidation by electrogenerating oxidizing species at the electrode materials surface (Sirés et al. 2014). The first mode occurs

less frequently due to its more specific oxidation behavior, since many organic pollutants are not electroactive. The indirect oxidation mode is generally considered as the main degradation and mineralisation mechanisms for electrochemical treatment of wastewater. Both anode and cathode can play a role in this oxidation process, according to their overvoltage values – also known as overpotential values – for oxygen evolution and hydrogen evolution, respectively (Figure 1) (Panizza and Cerisola 2009; Comninellis and Chen 2010; Mousset and Zhou 2017). The anode materials can be divided into two categories: (i) the active anodes that have a low overvoltage for O_2 evolution usually considered below 1.9 V; this is the case of dimensionally stable anode (DSA®) like RuO_2-IrO_2 with 1.4-1.7 V and platinum (Pt) in the range of 1.6-1.9 V, (ii) the non-active anodes that have a high O_2 evolution overvoltage usually considered higher than 1.9 V; this is the case of lead dioxide (PbO_2) with 1.8-2.0 V, tin oxide (SnO_2) with 2.0-2.2 V, sub-stoichiometric titanium oxide (Ti_xO_{2x-1} ($4 \leq x \leq 9$)) referred as TiO_x ($x < 2$) in this chapter (2.4-2.8 V), and boron-doped diamond with 2.2-2.8 V (Panizza and Cerisola 2009; Comninellis and Chen 2010). The oxidation involving at active anode materials is referred to electro-oxidation in this book chapter. In contrast to the active anodes, high O_2 overvoltage materials favor the generation of physisorbed $^{\bullet}OH$ radicals at their surface by water (H_2O) oxidation (Panizza and Cerisola 2009). This weak sorption makes $^{\bullet}OH$ radical available for matrix oxidation through the following reactions (Eqs. 1a-1b) at the anode (M) surface material (Panizza and Cerisola 2009):

$$M + H_2O \rightarrow M(^{\bullet}OH) + H^+ + e^- \quad (1a)$$

$$M(^{\bullet}OH) + \text{compounds} \rightarrow M + \text{oxidation products} \quad (1b)$$

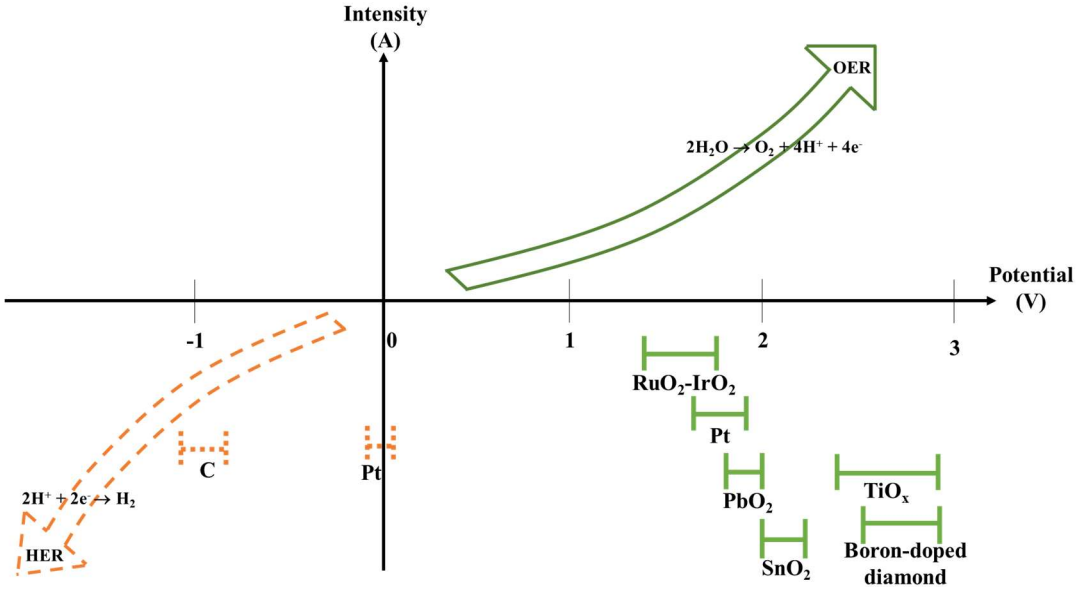

Figure 1. Overvoltage for hydrogen evolution at cathode (dashed line) and oxygen evolution at anode (full line) materials. OER occurs at the highest potentials using boron-doped diamond and TiO_x anodes, which makes them having a high oxidation power. HER occurs at low potential with carbon-based cathodes, which permit the electro-generation of H_2O_2 at their surface. Abbreviations: HER: hydrogen evolution reaction, OER: oxygen evolution reaction.

The non-active anodes are preferentially employed due to their benefit that can be obtained from the $^{\bullet}OH$ production and the subsequent high organic pollutant removal efficiency in an advanced electro-oxidation technology, that will be referred as anodic oxidation in this chapter. PbO_2 is a cheap material but has been put aside to avoid the possible release of toxic Pb^{2+} ions, though more recent studies highlight the development of more stable PbO_2-based anode (Panizza and Cerisola 2009; Aquino et al. 2014). Boron-doped diamond is the most widely used anode material in advanced electro-oxidation treatment for its high efficiency and good stability and resistance (Comninellis and Chen 2010; Brillas and Martinez-Huitle 2011). However, its relatively high cost makes its application limited to quite small treatment plants. TiO_x ($x < 2$) is gaining interest for its lower cost and its flexibility (Ganiyu et al. 2016, 2017). Though SnO_2 materials have currently a low stability for wastewater treatment application (Panizza and Cerisola 2009), its transparency makes it very interesting for hybrid photoelectrochemical processes (Mousset et al. 2017a) as discussed in sub-section 3.4.

The cathode materials can also participate in the oxidation mechanism according to their hydrogen (H_2) evolution overvoltage properties (Figure 1). A high H_2 overvoltage can promote the electrogeneration of hydrogen peroxide (H_2O_2) through the two-electron O_2 reduction reaction (Brillas et al. 2009):

$$O_2 + 2H^+ + 2e^- \rightarrow H_2O_2 \quad (2)$$

Platinum (Pt) is chemically inert in the electrochemical advanced oxidation processes' operating conditions and is useful for mechanism understanding studies. Though it has been widely employed at laboratory scale, Pt material is not only expensive but also not efficient to produce H_2O_2 (Sopaj 2013). Stainless steel is comparatively a cheap metal material, but the amount of electrogenerated H_2O_2 is still very low (Sopaj 2013; Mousset et al. 2018a).

Carbon materials have been preferentially studied in the electrochemical advanced oxidation processes area for their high H_2 overvoltage as well as high stability, high flexibility and low cost (Brillas et al. 2009; Chaplin 2014). Graphite represents an abundant natural form of carbon

and is therefore a cheap carbon material. However, its low specific surface area does not permit significant level of H_2O_2 concentration (Mousset et al. 2016d). The three-dimensional structure of felt form of carbon-based cathode has been widely investigated for its high specific surface area that allows the fast reduction of Fe^{3+} into Fe^{2+} (Eq. 3) (Sirés et al. 2007).

$$Fe^{3+} + e^- \rightarrow Fe^{2+} \quad (3)$$

This regeneration reaction permits the continuous production of $^{\bullet}OH$ radicals through Fenton reaction (Eq. 4) implemented in the so-called homogeneous electro-Fenton process when Fe^{2+} is dissolved or present initially in solution (Brillas et al. 2009; Mousset et al. 2016b):

$$H_2O_2 + Fe^{2+} \rightarrow Fe^{3+} + {}^{\bullet}OH + HO^- \quad (4)$$

Heterogeneous electro-Fenton processes that involve a source of iron, e.g. FeS_2 and Fe_3O_4, coated on the cathode material are emerging (Ganiyu et al. 2018). It avoids the pH adjustment to 3 unlike in homogeneous Fenton-based technology in which the dissolved Fe^{3+} would precipitate in $Fe(OH)_3$ otherwise. Sacrificial iron or steel anode materials have been widely employed as an alternative source of Fe^{2+} in peroxi-coagulation process (Brillas et al. 1997, 2003; Ren et al. 2018; Nidheesh 2018). Peroxi-coagulation consists of the combination of electro-Fenton that electro-generate H_2O_2 at cathode and electro-coagulation to produce Fe^{2+} by anodic dissolution.

Gas diffusion electrodes using carbon-polytetrafluoroethylene have been also suggested as carbon-based cathode material (Brillas et al. 2009). The O_2 flows through the thin and the porous carbon material, which enhances the O_2 transfer towards the cathode and therefore the yield of H_2O_2 electrogeneration (Sirés et al. 2007; Brillas et al. 2009; Martínez-Huitle et al. 2015). One drawback of gas diffusion electrodes cathodes is their low specific surface area that limits the rate of Fe^{2+} regeneration as compared to three dimensional carbon-based materials (Sirés et al. 2007). Some efforts have been made to enhance the specific surface area of carbon materials, including thermal treatment (Le et al. 2016), chemical treatment (Zhou et al. 2014) and graphene-doped modifications (Garcia-Rodriguez et al., 2018; Le et al., 2015a, 2015b; Mousset et al., 2017b, 2016c), with encouraging results for both H_2O_2 electrogeneration and Fe^{2+} regeneration.

2.2. Selection of photocatalyst for photocatalytic oxidation

Photocatalysis has been widely developed the last few decades as an alternative to traditional chemical advanced oxidation processes, by benefitting from the light to produce strong oxidizing agents like $^{\bullet}OH$ radicals using a catalyst (Fujishima et al. 2000; Malato et al. 2009; Lazar et al. 2012; Pelaez et al. 2012; Schneider et al. 2014). This photocatalyst is a semi-conductor that possess an energy gap region known as bandgap. Photocatalyst excitation with energy higher (i.e., light irradiation at a specific wavelength) than the bandgap promotes an excited electron into the conduction band (e_{cb}^-) leaving behind a positive vacancy namely as a hole (h_{vb}^+) (Eq. 5) that can then oxidize water (H_2O) (Eq. 6) or hydroxide ion (OH^-) (Eq. 7) to produce $^{\bullet}OH$ radicals.

$$\text{Photocatalyst} + h\nu \rightarrow e_{cb}^- + h_{vb}^+ \quad (5)$$

$$h_{vb}^+ + H_2O \rightarrow {}^{\bullet}OH + H^+ \quad (6)$$

$$h_{vb}^+ + OH^- \rightarrow {}^{\bullet}OH + H^+ \quad (7)$$

Among the numerous photocatalysts that have been tested in literature, titanium dioxide (TiO_2) is the most common material employed. The band gap for its anatase crystal phase is 3.2 eV, meaning that ultraviolet - noted UV in this chapter - radiation bellow 387 nm is required to initiate photocatalysis process. These UV-based photocatalysis are energy-consuming processes. Thus, numerous efforts have been devoted to benefit from the use of free solar light that is composed of 40% of visible light, in wavelength ranging from 400 nm to 800 nm. In this context, several visible light active photocatalysts have been proposed in literature with reduced band gap, including modified TiO_2 (Pelaez et al. 2012; Ding et al. 2012, 2014; Andersen et al. 2014; Barndõk et al. 2016; Fagan et al. 2016).

The photocatalysis can be implemented through two ways, either the photocatalyst is in suspension in the effluent to be treated or it is immobilized on a substrate. The first version allows for a higher surface of contact between the catalyst and the photons per unit volume, which can increase the quantum yield (Stefan 2017). However, a further separation stage is required in the treatment since the catalyst has to be recovered before the release of treated wastewater. Therefore, a preliminary catalyst immobilisation step is alternatively considered (Stefan 2017). The catalyst support is then another parameter to take into account for a good coating stability. A further advantage is that conductive substrate could bring synergy when combining electrochemical treatment with heterogeneous photocatalysis as discussed in section 2.3.

2.3. Selection of the catalyst support for electrocatalytic and photocatalytic oxidation combination

According to the following criteria, different processes can be implemented or not, i.e. electrochemical treatments or not, and/or photochemical processes or not, and/or photo-electrochemical combinations (Table 1):

(1) presence or not of electrode, involvement or not of high overvoltage electrode

(2) presence of light or not, presence of photocatalyst or not, presence of photocatalyst on electrode or not

Table 1. Implementation of electrolysis, photochemical processes and possible combinations between electrolysis and photochemistry, depending on criteria involved. According to the kind of combination, the processes implemented can vary from a simple photolysis or electro-oxidation to a more complex system combining electrochemical advanced oxidation processes with photoelectrocatalysis.

	Absence of light	**Light without catalyst**	**Light with photocatalyst not coated on electrode**	**Light with photocatalyst coated on electrode**
Absence of electrode	∅	Photolysis	Photocatalysis	∅
Absence of high overvoltage electrode	Electro-oxidation	Electro-oxidation/ photolysis	Electro-oxidation/ photocatalysis	Photoelectrocatalysis
High overvoltage electrode	Electro-chemical advanced oxidation processes	Electrochemical advanced oxidation processes/ photolysis	Electrochemical advanced oxidation processes/ photocatalysis	Electrochemical advanced oxidation processes/ photoelectrocatalysis

The possible combinations highlight a possible increase of electrocatalytic activity accompanying by a possible increase of photocatalytic activity according to the criteria involved. The increase of catalytic activity leads to higher number of •OH production sites as it has been previously proposed in literature (Brillas et al., 2009; Goldstein et al., 2007; Luo et al., 2015; Mousset et al., 2017a; Sun and Pignatello, 1993), which is summarized in Table 2 and displayed in Figure 2.

As represented in Table 2 and Figure 2, the electro-oxidation process does not bring any source of •OH production, since only direct oxidation occurs. When electro-oxidation is combined to

299 photolysis (electro-oxidation/photolysis), there is no •OH production as well, since only
300 photosensitive pollutants are degraded by photolysis. In electro-oxidation/photocatalysis the
301 •OH production site is coming from the photocatalysis itself as explained in sub-section 2.2.
302 Similarly, photoelectrocatalysis lead to the generation of one •OH site. Still, a difference of
303 oxidation efficiency can be observed between photocatalysis and photoelectrocatalysis
304 processes. An important waste reaction occurs during the photocatalysis mechanism, which
305 consists on the electron/hole pair recombination (Eq. 8) (Schneider et al. 2014):

306 $e_{cb}^- + h_{vb}^+ \rightarrow$ Photocatalyst + heat (8)

307

Table 2. Number of •OH production sites according to the kind of combination between electrolysis and photochemical processes. There is no •OH production in electro-oxidation system combined with photolysis. Implementing photocatalysis or photoelectrocatalysis results in increasing the number of •OH production site by one. The number of •OH production site drastically increases when electrochemical advanced oxidation processes such as anodic oxidation and/or electro-Fenton are involved. Their combination with photolysis or photocatalysis/photoelectrocatalysis increases even higher the number of •OH production site due to synergy. Abbreviations: AO: anodic oxidation, EA-H_2O_2: H_2O_2 electro-activation, EO: electro-oxidation, H_2O_2-$O_2^{-\bullet}$: H_2O_2 reaction with $O_2^{-\bullet}$, PL: photolysis, PC: photocatalysis, PEC: photoelectrocatalysis.

Electrochemical process	**Photochemical process**		
	Photolysis ($0 \times$ •OH)	**Photocatalysis** ($1 \times$ •OH)	**Photoelectrocatalysis** ($1 \times$ •OH)
Electro-oxidation ($0 \times$ •OH)	$(0 \times \bullet OH)_{PL}$ + $(0 \times \bullet OH)_{EO}$ **= 0 × •OH**	$(1 \times \bullet OH)_{PC}$ + $(0 \times \bullet OH)_{EO}$ **= 1 × •OH**	$(1 \times \bullet OH)_{PC}$ + $(0 \times \bullet OH)_{EO}$ **= 1 × •OH**
H_2O_2 electro-activation ($1 \times$ •OH)	$(0 \times \bullet OH)_{PL}$ + $(1 \times \bullet OH)_{EA\text{-}H2O2}$ + $(1 \times \bullet OH)_{synergyPL/EA\text{-}H2O2}$ **= 2 × •OH**	$(1 \times \bullet OH)_{PC}$ + $(1 \times \bullet OH)_{EA\text{-}H2O2}$ + $(1 \times \bullet OH)_{synergyPL/EA\text{-}H2O2}$ + $(1 \times \bullet OH)_{H2O2\text{-}O2\text{-}\bullet}$ **= 4 × •OH**	$(1 \times \bullet OH)_{PC}$ + $(1 \times \bullet OH)_{EA\text{-}H2O2}$ + $(1 \times \bullet OH)_{synergyPL/EA\text{-}H2O2}$ + $(1 \times \bullet OH)_{H2O2\text{-}O2\text{-}\bullet}$ **= 4 × •OH**
Anodic oxidation ($1 \times$ •OH)	$(0 \times \bullet OH)_{PL}$ + $(1 \times \bullet OH)_{AO}$ **= 1 × •OH**	$(1 \times \bullet OH)_{PC}$ + $(1 \times \bullet OH)_{AO}$ **= 2 × •OH**	$(1 \times \bullet OH)_{PC}$ + $(1 \times \bullet OH)_{AO}$ **= 2 × •OH**
Electro-Fenton ($2 \times$ •OH)	$(0 \times \bullet OH)_{PL}$ + $(1 \times \bullet OH)_{EF}$ + $(1 \times \bullet OH)_{EA\text{-}H2O2}$ + $(1 \times \bullet OH)_{synergyPL/EA\text{-}H2O2}$ + $(1 \times \bullet OH)_{synergyPL/EF}$ **= 4 × •OH**	$(1 \times \bullet OH)_{PC}$ + $(1 \times \bullet OH)_{EF}$ + $(1 \times \bullet OH)_{EA\text{-}H2O2}$ + $(1 \times \bullet OH)_{synergyPL/EA\text{-}H2O2}$ + $(1 \times \bullet OH)_{synergyPL/EF}$ + $(1 \times \bullet OH)_{H2O2\text{-}O2\text{-}\bullet}$ **= 6 × •OH**	$(1 \times \bullet OH)_{PC}$ + $(1 \times \bullet OH)_{EF}$ + $(1 \times \bullet OH)_{EA\text{-}H2O2}$ + $(1 \times \bullet OH)_{synergyPL/EA\text{-}H2O2}$ + $(1 \times \bullet OH)_{synergyPL/EF}$ + $(1 \times \bullet OH)_{H2O2\text{-}O2\text{-}\bullet}$ **= 6 × •OH**
Electro-Fenton/anodic oxidation ($4 \times$ •OH)	$(0 \times \bullet OH)_{PL}$ + $(1 \times \bullet OH)_{EF}$ + $(1 \times \bullet OH)_{AO}$ + $(1 \times \bullet OH)_{EA\text{-}H2O2}$ + $(1 \times \bullet OH)_{synergyEF/AO\text{-}peroxone}$ + $(1 \times \bullet OH)_{synergyPL/EA\text{-}H2O2}$ + $(1 \times \bullet OH)_{synergyPL/EF}$ **= 6 × •OH**	$(1 \times \bullet OH)_{PC}$ + $(1 \times \bullet OH)_{EF}$ + $(1 \times \bullet OH)_{AO}$ + $(1 \times \bullet OH)_{EA\text{-}H2O2}$ + $(1 \times \bullet OH)_{synergyEF/AO\text{-}peroxone}$ + $(1 \times \bullet OH)_{synergyPL/EA\text{-}H2O2}$ + $(1 \times \bullet OH)_{synergyPL/EF}$ + $(1 \times \bullet OH)_{H2O2\text{-}O2\text{-}\bullet}$ **= 8 × •OH**	$(1 \times \bullet OH)_{PC}$ + $(1 \times \bullet OH)_{EF}$ + $(1 \times \bullet OH)_{AO}$ + $(1 \times \bullet OH)_{EA\text{-}H2O2}$ + $(1 \times \bullet OH)_{synergyPL/EA\text{-}H2O2}$ + $(1 \times \bullet OH)_{synergyPL/EF}$ + $(1 \times \bullet OH)_{synergyEF/AO\text{-}peroxone}$ + $(1 \times \bullet OH)_{H2O2\text{-}O2\text{-}\bullet}$ **= 8 × •OH**

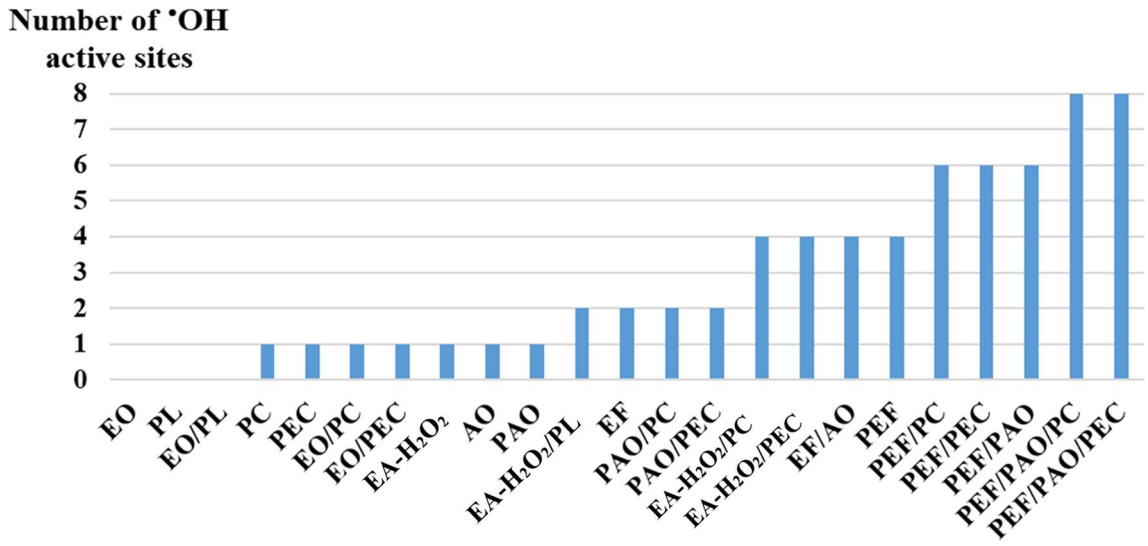

Figure 2. Number of •OH active sites according to the single and combined processes implemented. The combination giving the maximum number of •OH production site, i.e. eight production sites, is photoelectro-Fenton with photoanodic oxidation and photocatalysis or photoelectrocatalysis. Abbreviations: AO: anodic oxidation, EA-H_2O_2: H_2O_2 electro-activation, EO: electro-oxidation, PAO: photoanodic oxidation, PC: photocatalysis, PEC: photoelectrocatalysis, PEF: photoelectro-Fenton, PL: photolysis.

In photoelectrocatalysis, the photocatalyst is coated on a conductive material that can be used as an electrode in the electrolysis process (Catanho et al. 2006; Esquivel et al. 2009; Liu et al. 2009; Ding et al. 2012; Daskalaki et al. 2013; Garcia-Segura et al. 2013; Zhai et al. 2013; Ramirez et al. 2015; Bessegato et al. 2015). This configuration has the advantage to reduce the charge recombination (Zhai et al. 2013; Bessegato et al. 2015), as depicted in Figure 3. This enhances the degradation and mineralisation efficiency as demonstrated previously by Ding et al. (2012) who noticed a 2.5 times increase of degradation rate with photoelectrocatalysis-based process as compared to photocatalysis technology. This synergistic effect can be ascribed to the transfer of photo-electrons to the cathode that enhance the electro-generation of H_2O_2 for electro-Fenton process while limiting the charge recombination in photocatalysis mechanism (Ding et al. 2012).

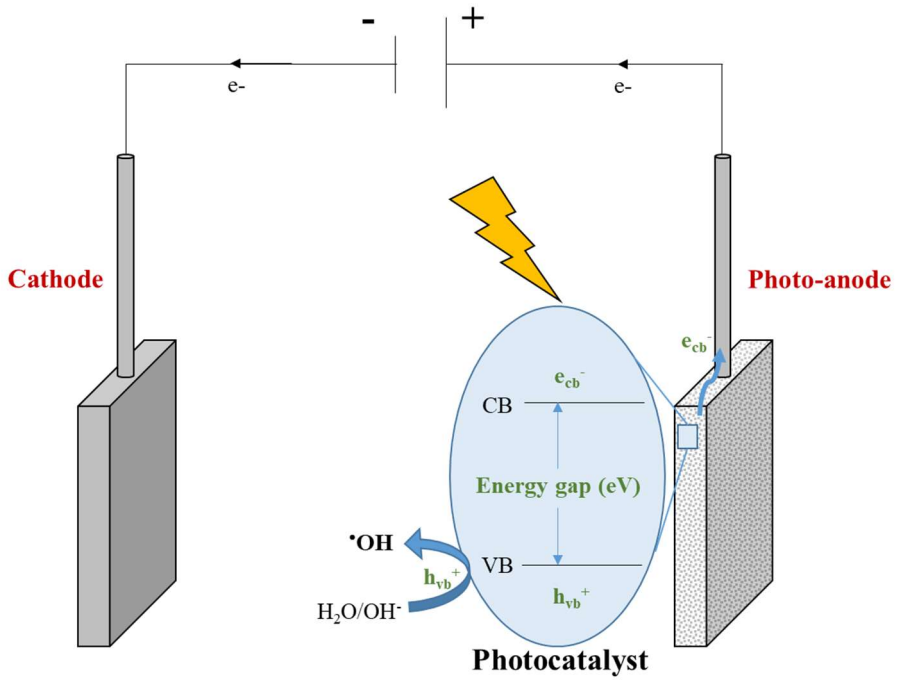

Figure 3. Photoelectrocatalysis process combining the electrolysis with a photo-anode. The advantage of this system compared to photocatalysis is that it limits the charge recombination, i.e. e_{cb}^- and h_{vb}^+, since the electron (e_{cb}^-) is driven to the cathode. Abbreviations: CB: conductive band, e_{cb}^-: electron in the conduction band, h_{vb}^+: positive vacancy (hole) in the valence band, VB: valence band.

In the presence of the cathodic generation of H_2O_2, it has recently been demonstrated that •OH radicals could be formed through electro-activation of H_2O_2 with one electron (Eq. 9) (Luo et al. 2015):

$$H_2O_2 + e^- \rightarrow {}^{\bullet}OH + HO^- \quad (9)$$

When H_2O_2 electro-activation is combined with photocatalysis or photoelectrocatalysis, a synergy could be observed with the H_2O_2 photolysis under UVC irradiation ($\lambda < 280$ nm) by homolytic cleavage giving another source of •OH (Eq. 10) (Goldstein et al. 2007):

$$H_2O_2 + h\nu \rightarrow 2\ {}^{\bullet}OH \quad (10)$$

Anodic oxidation process combined with photolysis – referred as photoanodic oxidation in this chapter – cannot bring another production site of •OH (Table 2). Interestingly, electro-Fenton can bring synergy in electro-Fenton/photolysis combination, namely photoelectro-Fenton process, through the UV irradiation of Fe(III)-monohydroxy complex ($Fe(OH)^{2+}$) that

represents an additional $^{\bullet}OH$ production source (Eqs. 11a-11b) (Sun and Pignatello 1993; Brillas et al. 2009):

$$H_2O + Fe^{3+} \leftrightarrow Fe(OH)^{2+} + H^+ \quad (11a)$$

$$Fe(OH)^{2+} + h\nu \rightarrow Fe^{2+} + {}^{\bullet}OH \quad (11b)$$

$Fe(OH)^{2+}$ is the predominant Fe(III) species at pH around 3 (Faust and Hoigné 1990), which corresponds to the optimal pH for electro-Fenton process (Brillas et al. 2009; Mousset et al. 2016e). Therefore, the production rate of $Fe(OH)^{2+}$ is not negligible and indirectly the $^{\bullet}OH$ production as well. In addition, the UV light allow the regeneration of Fe^{2+} in the meanwhile from Eq. 11b.

It is critical to underline that $^{\bullet}OH$ is not the sole oxidant that can participate in the organic removal efficiency. Mediated oxidation can also occur during the photoelectrochemical processes, by the production of weaker oxidants such as some reactive oxygen species like superoxide anion ($O_2^{-\bullet}$) (Eq. 12) in photocatalysis and photoelectrocatalysis processes and ozone (O_3) (Eq. 13) with non-active anodes in anodic oxidation technology (Bergmann et al. 2009; dos Santos and Scialdone 2018):

$$e_{cb}^- + O_2 \rightarrow O_2^{-\bullet} \quad (12)$$

$$3H_2O \rightarrow O_3 + 6H^+ + 6e^- \quad (13)$$

Furthermore, depending on the characteristic of the effluent to treat and/or on the supporting electrolyte that is potentially added, the presence of chloride ion (Cl^-), sulfate ion (SO_4^{2-}), phosphate ion (PO_4^{3-}), and carbonate ion (CO_3^{2-}) can lead to the formation of radical species such as $Cl^{\bullet}$ (Eq. 14), $SO_4^{-\bullet}$ (Eq. 15), $PO_4^{2-\bullet}$ (Eq. 16), $CO_3^{-\bullet}$ (Eq. 17), respectively (Sirés et al. 2014):

$$Cl^- \rightarrow Cl^{\bullet} + e^- \quad (14)$$

$$SO_4^{2-} \rightarrow SO_4^{-\bullet} + e^- \quad (15)$$

$$PO_4^{3-} \rightarrow PO_4^{2-\bullet} + e^- \quad (16)$$

$$CO_3^{2-} \rightarrow CO_3^{-\bullet} + e^- \quad (17)$$

More stable oxidants can be generated from these radical species (Cl_2 (Eq. 18), $S_2O_8^{2-}$ (Eq. 19), $P_2O_8^{4-}$ (Eq. 20), $C_2O_6^{2-}$ (Eq. 21)) (Moreira et al. 2017):

$$2\,Cl^{\bullet} \rightarrow Cl_2 \quad (18)$$

$2\ SO_4^{-\bullet} \rightarrow S_2O_8^{2-}$ (19)

$2\ PO_4^{2-\bullet} \rightarrow P_2O_8^{4-}$ (20)

$2\ CO_3^{-\bullet} \rightarrow C_2O_6^{2-}$ (21)

Under light irradiation, Cl_2 and $S_2O_8^{2-}$ can generate $Cl^{\bullet}$ (Eqs. 22a-22b) and $SO_4^{-\bullet}$ (Eq. 23), respectively (dos Santos and Scialdone 2018):

$Cl_2 + H_2O \rightarrow HClO + Cl^- + H^+$ (22a)

$HClO + h\upsilon \rightarrow Cl^{\bullet} + {}^{\bullet}OH$ (22b)

$S_2O_8^{2-} + h\upsilon \rightarrow 2SO_4^{\bullet}$ (23)

This mediated oxidation can also lead to additional production source of ${}^{\bullet}OH$ through peroxone equation (Eq. 24) and H_2O_2 reaction with $O_2^{-\bullet}$ (Eq. 25) (Brillas et al. 2009; Merényi et al. 2010):

$H_2O_2 + 2O_3 \rightarrow 2{}^{\bullet}OH + 3O_2$ (24)

$H_2O_2 + O_2^{-\bullet} \rightarrow {}^{\bullet}OH + OH^- + O_2$ (25)

However, mediated oxidants such as chlorinated ones can lead to toxic inorganic, e.g. chlorate (ClO_3^-) and perchlorate (ClO_4^-), and organic intermediates such as trihalomethanes (THMs) and chloroform that accumulate in solution (Araújo et al. 2015; Brito et al. 2015; Mousset et al. 2018b, 2020). It is therefore important to control their concentration and to adapt the operating conditions in order to limit their formation.

Interestingly, the combination that could give theoretically the highest number of ${}^{\bullet}OH$ production sites, i.e. 8 production sites, is photoelectro-Fenton with photoanodic oxidation and photocatalysis or photoelectrocatalysis, i.e. photoelectro-Fenton/photoanodic oxidation/photocatalysis or photoelectro-Fenton/photoanodic oxidation/photoelectrocatalysis respectively (Mousset et al. 2017a), as schematically presented in Figure 4.

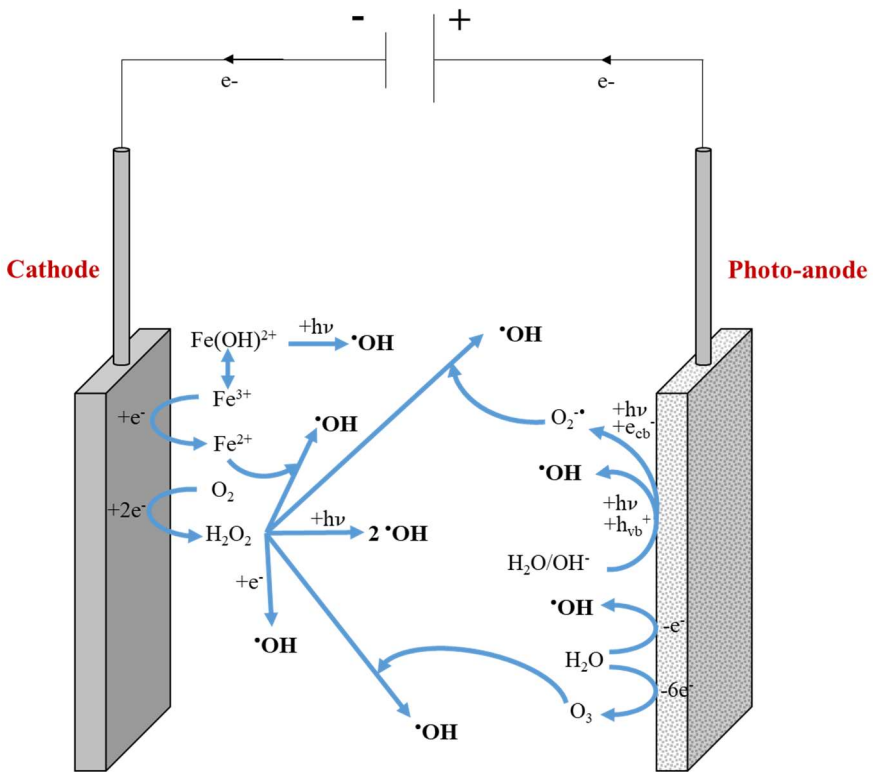

Figure 4. Different •OH production sites in the photoelectro-Fenton/photoanodic oxidation/photoelectrocatalysis process combining electrochemical advanced oxidation processes with photoelectrocatalysis. There is a maximum of eight •OH production sites from eight different reactions involved at the photo-anode, at the cathode and in the bulk solution. It is important to highlight that the occurrence of these reactions is depending on the solution pH, the applied wavelength, and the production rate of reagent such as H_2O_2 involved in parallel reactions.

It is important to emphasize the fact that a higher number of •OH production sites does not systematically mean that the oxidation efficiency will be better. There can be kinetic competitions with reactions requiring the same reagents to produce •OH radicals. For instance, H_2O_2 is involved in Fenton reaction (Eq. 4) but also in H_2O_2 electro-activation (Eq. 9), in H_2O_2 photolysis (Eq. 10), in peroxone equation (Eq. 24) and in reaction with $O_2^{-\bullet}$ (Eq. 25), meaning that the •OH production yield will not be automatically increased through five production sites instead of one at constant electrogeneration of H_2O_2, the rate of H_2O_2 production being the limiting step (Mousset et al. 2017a).

Moreover, some side reactions that consume •OH can limit its action (dos Santos and Scialdone 2018):

$$SO_4^{-\bullet} + {}^{\bullet}OH \rightarrow HSO_4^- + \tfrac{1}{2}O_2 \quad (26)$$

$$^{\bullet}OH + H_2O_2 \rightarrow H_2O + HO_2^{\bullet} \quad (27)$$

$Fe^{2+} + {}^{\bullet}OH \rightarrow Fe^{3+} + OH^{-}$ (28)

The reaction between Fe^{2+} and $^{\bullet}OH$ (Eq. 28) is particularly an important parasitic reactions in Fenton-based processes (Brillas et al. 2009; Mousset et al. 2016a). In addition, the solution pH can interfere in the number of $^{\bullet}OH$ production sites since the Fenton reaction is optimal at pH 3 in homogeneous systems (Brillas et al. 2009). In contrast, $O_2^{-\bullet}$ species is predominant at pH higher than 6.8, considering a pKa ($HO_2^{\bullet}/O_2^{-\bullet}$) equal to 4.8, and therefore the generation of $^{\bullet}OH$ through Eq. 25 is optimal at circumneutral pH (Mousset et al. 2018a). Implementing heterogeneous electro-Fenton process in combination to photoelectrocatalysis could solve this issue. The wavelength range of light irradiation also plays a role in the number of $^{\bullet}OH$ production sites. Thus, H_2O_2 photolysis mainly occurs under UVC irradiation ($\lambda < 280$ nm), while photocatalysis and photoelectrocatalysis are often performed using UVA (315 nm $< \lambda <$ 400 nm) and even visible light irradiation (400 nm $< \lambda <$ 800 nm). It should be emphasized that the synergy of combinations between H_2O_2 photolysis and photocatalysis or photoelectrocatalysis, i.e. in H_2O_2 electro-activation/photocatalysis, H_2O_2 electro-activation/photoelectrocatalysis, photoelectro-Fenton/photocatalysis, photoelectro-Fenton/photoelectrocatalysis, photoelectro-Fenton/photoanodic oxidation/photocatalysis, photoelectro-Fenton/photoanodic oxidation/photoelectrocatalysis, cannot occur if the photocatalyst does not absorb light under UVC irradiation and/or for economic reason if the system is operated under solar light. The organic load has an impact on the kinetics of degradation rates but should not hamper the number of $^{\bullet}OH$ production sites (Garcia-Segura et al. 2014). This is the case only if the turbidity is not impacted by the increase of organic load, otherwise the yields of UV-based reactions will be altered.

The combination of processes along with possible synergy can be optimized via reactor design that need to be adapted according to the reactions involved as discussed in section 3.

3. Reactor design

The reactor design is an important parameter to take into account in order to optimize the photo-electrochemical technologies. The existing combinations between electrolysis and

468 photocatalysis or photoelectrocatalysis technologies proposed in literature for wastewater
469 treatment application are presented in Table 3. The influence of criteria studied in literature
470 about the photo-electrochemical reactor design is presented in the following sub-sections 3.2,
471 3.3 and 3.4.
472

Table 3. Processes combination between electrolysis and photocatalysis or photoelectrocatalysis processes proposed in literature for wastewater treatment application. Different reactor designs have been proposed: sequential or hybrid reactors, divided or undivided cells, flow-cell or stirred tank reactor, external or immersed light source, light source positioned on the top or bottom or on the side of reactor, light source placed vertically or horizontally.

Processes implemented	**Reactor configuration**	**Cathode**	**Anode**	**Electrode positioning**	**Photocatalyst**	**Kind of light**	**Light source positioning**	**Reference**
Photoelectro-Fenton/photocatalysis	Undivided cell Cylindrical stirred tank photo-reactor	Boron-doped diamond	Boron-doped diamond	Both parallel and vertical	TiO_2 immobilized on glass spheres and horizontal nylon mesh	Solar light	Externally, on the top of the reactor	(Garza-Campos et al. 2014)
Photoelectro-Fenton/photocatalysis	Undivided cell Electrochemical flow-cell Sequential reactors (electrolyser→photoreactors) in recirculation	Carbon-polytetrafluoro-ethylene air diffusion cathode	Pt	Both parallel and vertical	TiO_2 immobilized on glass spheres	Solar light	Externally, on the top of the reactor	(Garza-Campos et al. 2016)
Photoelectro-Fenton/photocatalysis	Undivided cell Parallelepiped stirred tank photo-reactor	Graphite/Carbon nanotubes	Pt	Both parallel and vertical	TiO_2 immobilized on glass plates on vertical sides of the reactor	UV light	Immersed vertically in the reactor	(Khataee et al. 2012)
Photoelectro-Fenton/photoanodic oxidation/photocatalysis	Undivided cell Cylindrical glass stirred tank photo-reactor	Carbon felt	Glass/fluorine-doped tin oxide (transparent)	Both parallel and vertical	TiO_2 immobilized on cylindrical glass reactor	UV light	Externally, on the side of the reactor, close to the cathode	(Mousset et al. 2017a)
Photoelectrocatalysis	Undivided cell Cylindrical stirred tank photo-reactor	Ti/Ru	Boron-doped TiO_2 nanotubes	Both parallel and vertical	TiO_2	UV/Visible light	Immersed vertically in the reactor	(Bessegato et al. 2015)
Photoelectrocatalysis	Undivided cell Cylindrical quartz stirred tank photo-reactor	Pt	Carbon cloth/reduced graphene oxide/TiO_2	Both parallel and vertical	TiO_2	Visible light	Not specified	(Zhai et al. 2013)
Photoelectrocatalysis	Undivided cell Cylindrical stirred tank photo-reactor	Boron-doped diamond	Indium tin oxide/TiO_2	Anode: horizontal	TiO_2	Solar light	Externally, on the top of the reactor	(Daskalaki et al. 2013)

				(at the bottom) Cathode: vertical				
Photoelectrocatalysis	Undivided cell Cylindrical stirred tank photo-reactor	Carbon-polytetrafluoro-ethylene air diffusion cathode	Stainless steel/TiO_2	Anode: oblique Cathode: vertical	TiO_2	Solar light	Externally, on the top of the reactor	(Garcia-Segura et al. 2013)
Photoelectrocatalysis	Undivided cell Photo-electrochemical flow-cell	Ti mesh on a quartz plate (transparent)	$Ti/Ru_{0.3}Ti_{0.7}O_2$	Both parallel and vertical	$Ti_{0.7}O_2$	UV light	Externally, on the side of the reactor, close to the cathode	(Catanho et al. 2006)
Photoelectro-Fenton/ photoelectrocatalysis	Undivided cell Cylindrical quartz stirred tank photo-reactor	Reticulated vitreous carbon	Ti/TiO_2	Anode: horizontal (at the bottom) Cathode: vertical	TiO_2	UV/Visible light	Externally, at the bottom of the reactor	(Xie and Li 2006)
Photoelectro-Fenton/ photoelectrocatalysis	Divided cell Cylindrical quartz stirred tank photo-reactors	Carbon felt	Ti/TiO_2	Both parallel and vertical	TiO_2	UV light	Externally, on the side of the anodic compartment	(Ramirez et al. 2015)
Photoelectro-Fenton/ photoelectrocatalysis	Divided cell Cylindrical glass stirred tank photo-reactor	Carbon cloth	Antimony-doped tin oxide/Optical fibre/TiO_2 (transparent)	Both parallel and vertical	TiO_2	UV light	Immersed vertically in the reactor	(Esquivel et al. 2009)
Photoelectro-Fenton/photoanodic oxidation/ photoelectrocatalysis	Undivided cell semi-cylindrical quartz stirred tank photo-reactor	Activated carbon fibre/$Fe@Fe_2O_3$	Glass/fluorine-doped tin oxide/Bi_2WO_6 (transparent)	Both parallel and vertical; anode close to the flat side of the reactor	Bi_2WO_6 (visible light active)	Visible light	Externally, on the flat side of the reactor	(Ding et al. 2012)

3.1. Sequential versus hybrid reactors

There are two possibilities to consider the combination between photochemical and electrochemical processes combination. The first one is a configuration as sequential reactors with a possibility of recirculation of the effluent (Figure 5a). The photochemical process can be either positioned as primary treatment followed by the electrochemical process or in the reverse order. If a continuous system is considered without recirculation, the electrochemical technology has advantages to be placed first because the stable oxidizing species such as H_2O_2 formed by the electrode materials can then be photolysed in the photo process and produce $^{\bullet}OH$ radicals (Garcia-Segura and Brillas 2014; Garza-Campos et al. 2016). In the same way, the ferro-hydroxy complex formed in the electrolyser can also be photolysed in the subsequent photo-reactor (Garcia-Segura and Brillas 2014; Garza-Campos et al. 2016).

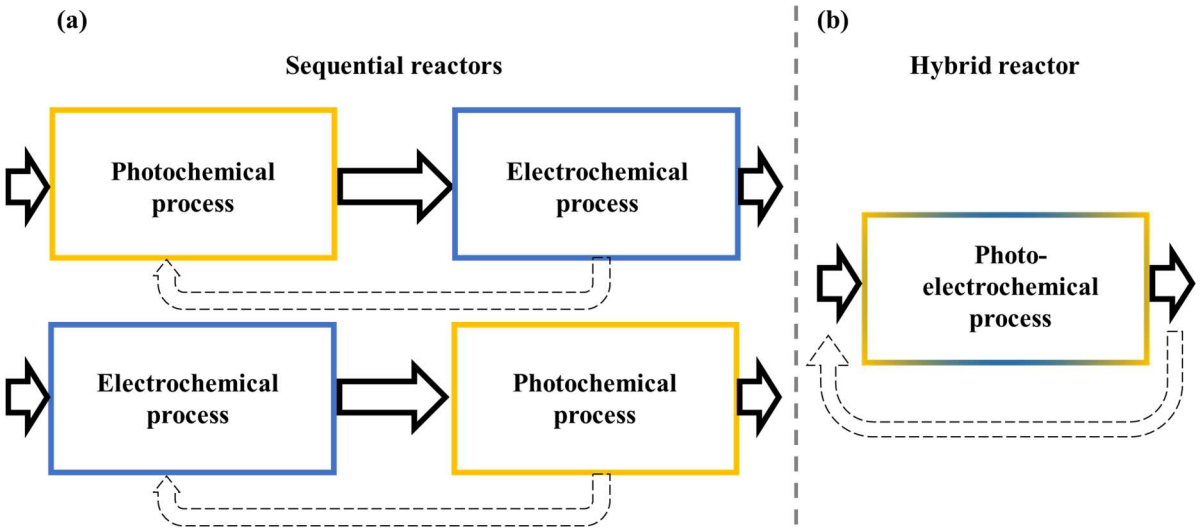

Figure 5. Sequential (a) versus hybrid (b) reactors for photochemical and electrochemical processes combination. In a continuous system an electrochemical process followed by a photochemical technology has the advantage to produce $^{\bullet}OH$ from the photolysis of some species such as H_2O_2 and ferro-hydroxy complex produced by electrolysis. A hybrid photo-electrochemical process leads to less footprint area and higher possibility of synergy between photochemical and electrochemical reactions.

In contrast, the hybrid photo-electrochemical process (Figure 5b) offers many other advantages such as the low footprint area, the possibility of synergy between photochemical and electrochemical reactions according to the catalyst support as discussed in section 2.3 and to the hybrid reactor configuration as shown in the following sub-sections 3.2, 3.3 and 3.4. These

benefits gained from the hybrid process explain the higher number of studies selecting this configuration (Table 3).

3.2. Reactor configuration: divided versus undivided cells

In electrolysis, there are two possibilities of operation, either in divided cell (Figure 6a) or in undivided cell (Figure 6b). Considering the photo-electrochemical process implementation, the main influence of efficiency comes from the electrochemical reactions. In divided cell, the advantage is that there is the possibility to avoid decomposition of oxidants at anode or cathode which increases the faradic yield (Esquivel et al. 2009; Ramirez et al. 2015). However, some redox reactions cannot be involved in the cell such as ferrous/ferric cycle that is useful for the Fe^{2+} regeneration (Eq. 3) in an electro-Fenton process for example. In contrast, this catalytic behaviour of iron species can be obtained in an undivided cell (Sirés et al. 2007). This latter configuration has been the most studied in photo-electrochemical reactors (Table 3), especially for its easier implementation at industrial scale if a stirred tank reactor is foreseen.

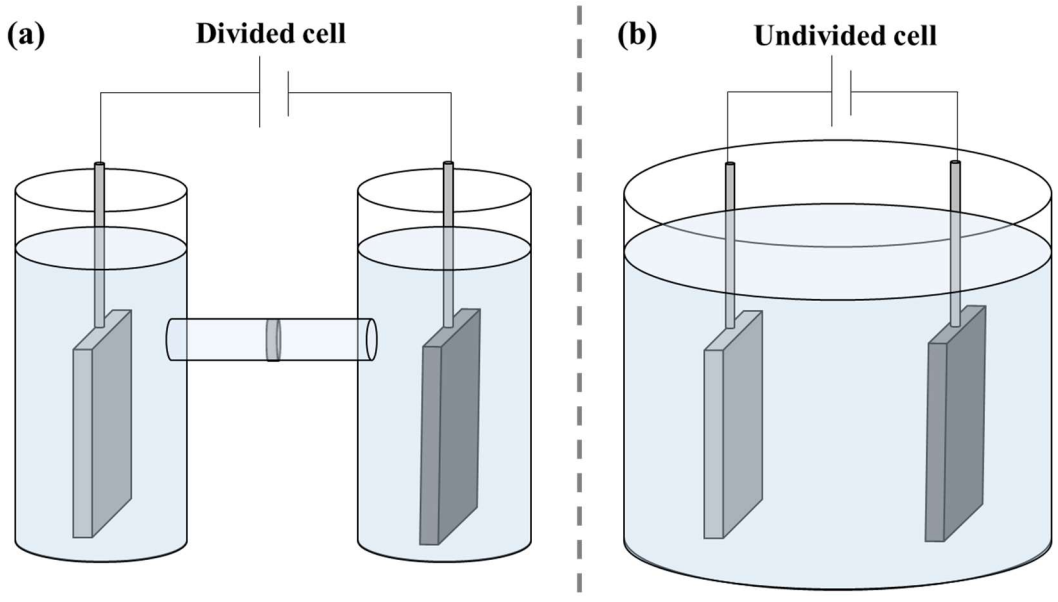

Figure 6. Divided cell (a) versus undivided cell (b) configurations for hybrid photo-electrochemical processes. Divided cell configuration avoids the decomposition of oxidants on the anode or cathode surfaces depending on the species. Practically, undivided cell is more developed and the redox cycle of iron can occur in this condition to implement Fenton reaction.

3.3. Operation mode: flow-cell versus stirred tank reactor

There are two main operation modes of photo-electrochemical reactors developed in literature (Figure 7). In the flow cell (Figure 7a), the flux is forced to go between parallel electrodes and the mode can be assimilated to a plug-flow reactor when flushed continuously. Most of the time it is operated in recirculated batch in lab scale studies. In a stirred tank reactor (Figure 7b), the electrodes are placed in parallel in a tank that is mechanically stirred (Ding et al. 2012; Zhai et al. 2013; Garcia-Segura et al. 2014; Bessegato et al. 2015; Mousset et al. 2017a). The effluent can be flushed continuously and can be ascribed to a continuous stirred tank reactor mode when the solution is assumed as perfectly mixed, i.e. the homogeneous concentration in the reactor equal the output stream.

A hydrodynamic characterisation has shown that parallel electrodes system in a stirred tank reactor could be modelled as an ideal single continuous stirred tank reactor at high rotational speed of the impeller with impeller Reynolds number higher than 10^4 (Polcaro et al., 2007). The geometry proposed in literature is either parallelepipedal (Khataee et al. 2012) or cylindrical (Ding et al. 2012; Zhai et al. 2013; Garcia-Segura et al. 2014; Bessegato et al. 2015; Mousset et al. 2017a). The latter is the most frequent shape since it limits the stagnant zone in which no mixing occurs. The drawbacks of continuous stirred tank reactor is that the mass transfer rate is lower than in flow cell (Anglada et al. 2010). This is confirmed by the comparison between a cylindrical stirred tank reactor of 0.1 L and a flow-by cell with a reservoir tank of 10 L that was performed by Garcia-Segura et al. (2014). Considering the difference of electrochemical reactor volume in each kind of reactor, the time to reach 50% of chloramphenicol degradation was 26-fold higher in stirred tank reactor than in solar filter-press reactor (Garcia-Segura et al. 2014).

Moreover, the electrode distance can be better controlled and easily optimized in flow cells by varying it from a few tens of microns until several centimetres (Scialdone et al. 2010). It leads to better mass transport of targeted compounds towards the electrodes, with mass transport coefficient improved by two to more than ten times (Anglada et al. 2010; Mousset et al. 2019b). A high mass transport is essential to favour heterogeneous catalysis (Mousset et al. 2019a) that is involved at electrode surface in photo-electrochemical processes. Minimized electrode distances also permit the reduction of cell potential and therefore the energy requirement is reduced. The flow cell has also advantage for process scale-up since it can be arranged in series and parallel to increase the removal efficiency and the treatment capacity respectively, while

keeping a low footprint compared to continuous stirred tank reactor (Martínez-Huitle et al. 2015).

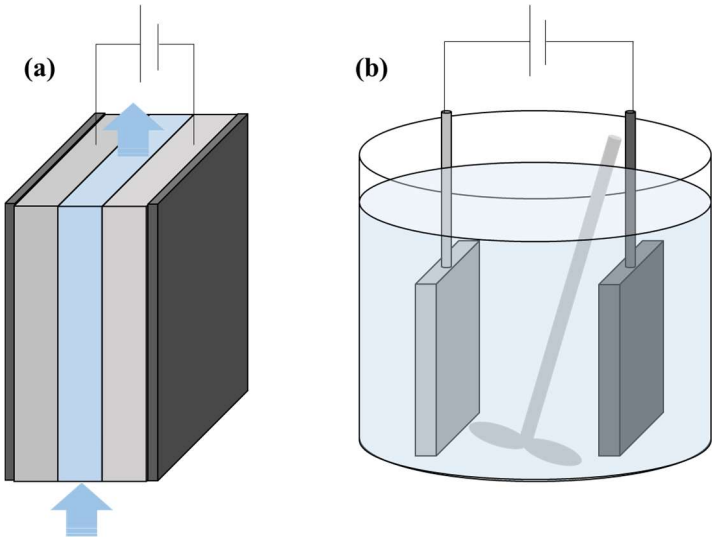

Figure 7. Flow-by cell (a) and stirred tank reactor (b) configurations for hybrid photo-electrochemical processes. The flow-by cell is assimilated to a plug-flow reactor while the stirred tank reactor is associated with the continuous stirred tank reactor model. The flow-by cell increases the mass transfers towards the electrodes compared to the stirred tank reactor, which is an advantage to implement heterogeneous catalysis and photochemical reactions.

3.4. Light source positioning

The light positioning is an important parameter in photochemical processes since the energy delivered by light irradiation decrease with the distance between the light source and the targeted compound in solution. The influence of light irradiation source placed in stirred tank reactor or in flow-cell configurations considering hybrid photo-electrochemical processes is displayed in Figure 8.

The light source can be placed externally of the reactor (Figures 8a-8g) and especially at the top of a stirred tank reactor with parallel electrode configuration (Garza-Campos et al. 2014) (Figure 8a) or with one vertical electrode and one horizontal electrode that contain the photocatalyst (Daskalaki et al. 2013) (Figure 8b) in order to improve the contact between the light and photocatalyst. In this latter case, the light can also be shined at the bottom of the stirred tank reactor (Xie and Li 2006) (Figure 8b) through the reactor in order to minimize the distance between the light and the horizontal photo-electrode. It is important to highlight that quartz reactors are preferred instead of glass reactors, since the transmittance of quartz material is very high for a wide range of wavelength, even in UV region (Mousset et al. 2017a).

553 Another possibility is to let shine the light across the side of the stirred tank reactor (Figure 8c)
554 and either enhance the H_2O_2 photolysis by being close to the carbon cathode (Mousset et al.
555 2017a) or improve the photoelectrocatalysis performance using a transparent photo-anode
556 (Mousset et al. 2017a). This latter option has been proposed to be implemented in a semi-
557 cylindrical reactor in which the transparent photo-anode is placed against the flat side (Ding et
558 al. 2012) (Figure 8d) in order to optimize the distance between the light and the photo-anode.
559 This distance is even better optimized in flow-cell systems in which interelectrode distance can
560 be easily reduced as discussed in section 3.3. In this configuration, the light is usually shined
561 through a mesh electrode (Catanho et al. 2006) (Figure 8e) or a transparent electrode (Figure
562 8f) using an external transparent wall.
563 More recently, it has been proposed to make full use of light energy by letting shine the light
564 directly across a transparent anode material (Mousset et al. 2017a) (Figure 8g), named fluorine-
565 doped tin oxide. This customized configuration could be obtained by additive manufacturing,
566 avoiding the use of quartz material that is expensive and fragile. The proposed three
567 dimensional-printed reactor design allowed for 1.87 times increase of efficiency of photo-based
568 processes involved in the reactor as compared to a continuous stirred tank reactor system.
569 Moreover, the use of fluorine-doped tin oxide offers the advantage of being a high O_2
570 overvoltage anode reaching a potential of 2.1 V (Mousset et al. 2017a), which constitutes
571 another source of $^{\bullet}OH$ production for electrochemical advanced oxidation processes
572 combination with photocatalysis or photoelectrocatalysis.
573
574 Immersed light positioning systems have also been considered (Bessegato et al., 2015; Esquivel
575 et al., 2009; Khataee et al., 2012) (Figures 8h, 8i). The source can be placed close to the cathode
576 and the anode in order to favour the photocatalysis mechanism combined with electrolysis
577 (Khataee et al. 2012; Bessegato et al. 2015) (Figure 8h). A second option is to use a source such
578 as optical fibre that is coated with a photocatalyst and employed as a photo-anode connected to
579 a cathode (Esquivel et al. 2009) (Figure 8i). In this latter case, the photoelectrocatalysis is
580 implemented and can be combined to electrochemical advanced oxidation processes
581 technologies for a better pollutant removal efficiency than electrochemical advanced
582 oxidation/photocatalysis processes combination, as discussed in section 2.3.
583 It is necessary to note that when a transparent material is used to involve photocatalysis or
584 photoelectrocatalysis in a light-through electrolytic system, there is an optimal photocatalyst
585 loading. It depends on several factors such as optical properties of the catalyst, e.g. optical

586 thickness and transmittance, and of the transparent substrate material as well as photocatalyst
587 particle size (Hurtado et al., 2015; Motegh et al., 2012; Murakami et al., 2012). For instance, it
588 has been shown that a transmittance of 20%, corresponding to a dose of 0.31 mg cm^{-2} of TiO_2
589 (P-25) coated on a glass/fluorine-doped tin oxide transparent material, was found optimal for a
590 maximum pollutant removal efficiency in a hybrid photo-electrochemical reactor (Mousset et
591 al. 2017a).
592
593 Another important point is that the use of solar light as irradiation source is decisive in the
594 position of electrodes in the reactor and in the reactor design as well. Since the solar light is
595 coming from the top, compound parabolic concentrators oriented towards the sun have been
596 developed to maximize the quantum yield and have been combined with electrolysis cells
597 (Garcia-Segura et al. 2014). Solar light was used as free energy source in photoelectrochemical
598 systems and could successfully reduce the operating costs while keeping very high removal
599 yield as compared to artificial light (El-Ghenymy et al. 2012, 2013; Garcia-Segura and Brillas
600 2014).

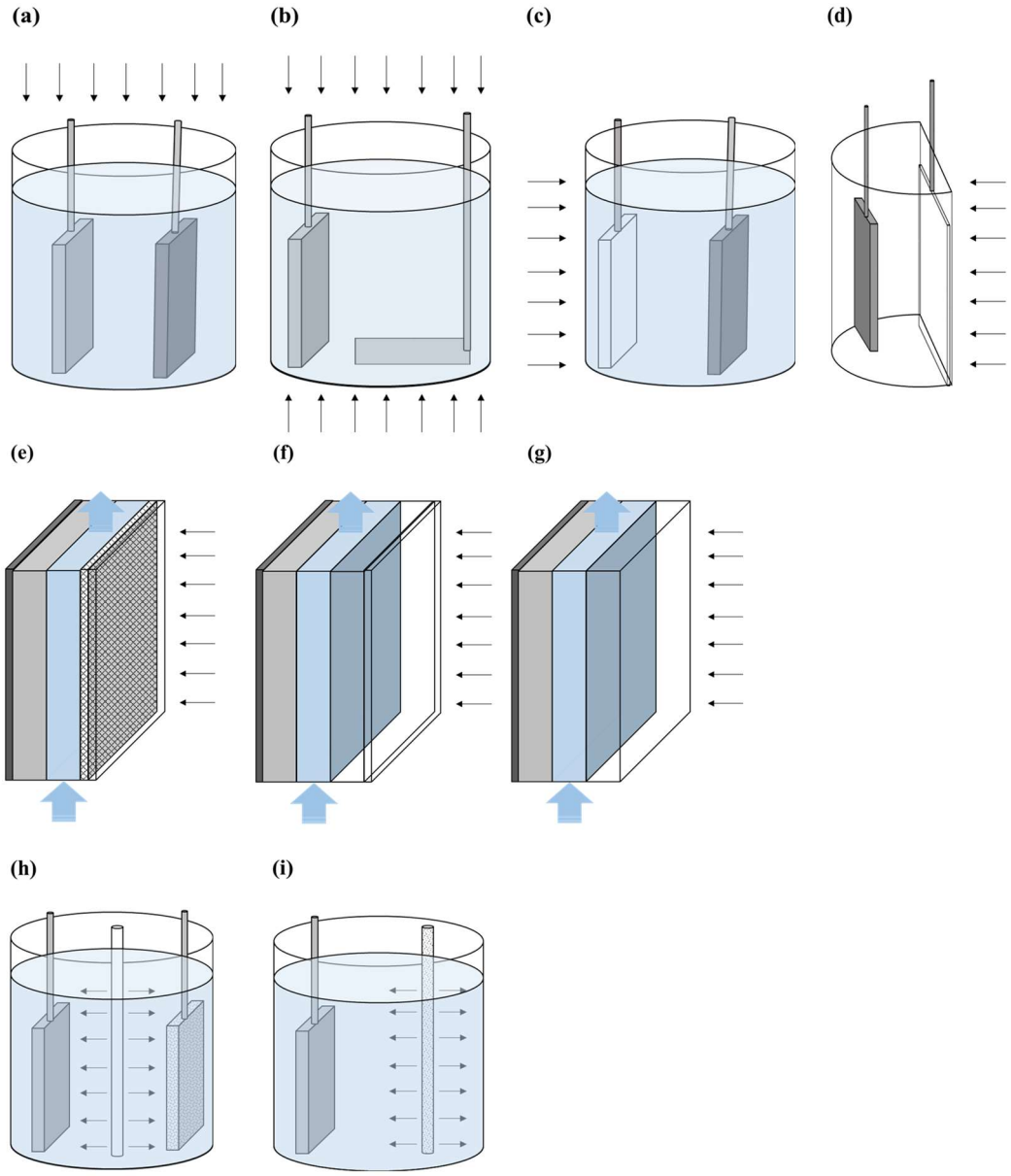

Figure 8. Influence of light irradiation source placed externally of the reactor ((a)-(g)) or immersed ((h), (i)), in stirred tank reactor ((a)-(d), (h), (i)) and in flow-cell ((e), (f), (g)) configurations considering hybrid photo-electrochemical processes. If an external source is implemented on the side or at the bottom of the reactor, the reactor material needs to be suitable for allowing UV radiation to pass through. Such material is quartz that is very fragile and expensive. When the light is implemented in a stirred tank reactor, the distance between the light source and the electrode needs to be minimized for better synergy and maximum quantum yields. Flow-cell allows varying the interelectrode gap from micro-distance (50-500 μm) to macro-distance (1-5 cm), which can easily permit optimisation of the penetration depth when light is applied through the cell.

4. Conclusion

Studies on photo-electrochemical reactors applied for advanced oxidation treatment of wastewater are still at early stages though increasing attention is being devoted to this technology. This chapter presented an overview of the possible synergetic combinations between advanced electrochemical treatments and photochemical processes. The effect of reactor design, i.e. sequential versus hybrid photo-reactors, divided versus undivided cells, operation mode, i.e. flow cell versus stirred tank reactors, and light source positioning, on the photo-reactors efficiency has been addressed. The synergy between photoelectrocatalysis and electrochemical advanced oxidation processes seems promising in terms of removal efficiency of organic pollutants.

Upon these preliminary results, there is a need to manufacture multifunctional electrode materials possessing optimum properties and configuration for the design/development of heterogeneous photocatalytic reactors with enhanced performance. In parallel, the photocatalysts have to be developed so they can possess long-term activity and improved coating stability, particularly when subjected to electric field.

Furthermore, most studies from literature are performed at laboratory scale while most of the effluents tested are synthetic solutions. There is a need to upscale those processes by testing real water matrix solutions. The pH, the temperature, the turbidity, the presence of organic matter as well as the inorganic salts could interfere with the combined process efficiency. A techno-economic study could then be assessed for comparison with commercialized technologies.

References

Alcántara MT, Gómez J, Pazos M, Sanromán MA (2009) PAHs soil decontamination in two steps: desorption and electrochemical treatment. J Hazard Mater 166:462–468. doi: 10.1016/j.jhazmat.2008.11.050

Almazán-Sánchez PT, Cotillas S, Sáez C, et al (2017) Removal of pendimethalin from soil washing effluents using electrolytic and electro-irradiated technologies based on diamond anodes. Appl Catal B Environ 213:190–197. doi: 10.1016/j.apcatb.2017.05.008

Andersen J, Han C, O'Shea K, Dionysiou DD (2014) Revealing the degradation intermediates and pathways of visible light-induced NF-TiO_2 photocatalysis of microcystin-LR. Appl

642 Catal B Environ 154–155:259–266. doi: 10.1016/j.apcatb.2014.02.025
643 Anglada A, Urtiaga AM, Ortiz I (2010) Laboratory and pilot plant scale study on the
644 electrochemical oxidation of landfill leachate. J Hazard Mater 181:729–35. doi:
645 10.1016/j.jhazmat.2010.05.073
646 Aquino JM, Rocha-Filho RC, Ruotolo LAM, et al (2014) Electrochemical degradation of a real
647 textile wastewater using β-PbO_2 and DSA® anodes. Chem Eng J 251:138–145. doi:
648 10.1016/j.cej.2014.04.032
649 Araújo DM de, Sáez C, Martínez-Huitle CA, et al (2015) Influence of mediated processes on
650 the removal of Rhodamine with conductive-diamond electrochemical oxidation. Appl
651 Catal B Environ 166–167:454–459. doi: 10.1016/j.apcatb.2014.11.038
652 Barndõk H, Hermosilla D, Han C, et al (2016) Degradation of 1,4-dioxane from industrial
653 wastewater by solar photocatalysis using immobilized NF-TiO_2 composite with
654 monodisperse TiO_2 nanoparticles. Appl Catal B Environ 180:44–52. doi:
655 10.1016/j.apcatb.2015.06.015
656 Bergmann MEH, Rollin J, Iourtchouk T (2009) The occurrence of perchlorate during drinking
657 water electrolysis using BDD anodes. Electrochim Acta 54:2102–2107. doi:
658 10.1016/j.electacta.2008.09.040
659 Besnault S, Martin S (2011) Etat de l'art sur les procédés avancés intensifs pour la réduction
660 de micropolluants dans les eaux usées traitées. Rapport bibliographique (French).
661 https://professionnels.afbiodiversite.fr/sites/default/files/pdf/2011_039.pdf
662 Bessegato GG, Cardoso JC, Zanoni MVB (2015) Enhanced photoelectrocatalytic degradation
663 of an acid dye with boron-doped TiO_2 nanotube anodes. Catal Today 240:100–106. doi:
664 10.1016/j.cattod.2014.03.073
665 Brillas E, Boye B, Dieng MM (2003) Peroxi-coagulation and photoperoxi-coagulation
666 treatments of the herbicide 4-chlorophenoxyacetic acid in aqueous medium using an
667 oxygen-diffusion cathode. J Electrochem Soc 150:E148–E154. doi: 10.1149/1.1543950
668 Brillas E, Martinez-Huitle CA (2011) Synthetic diamond films: preparation, electrochemistry,
669 characterization, and applications. Wiley, New Jersey. doi:10.1002/9781118062364
670 Brillas E, Martínez-Huitle CA (2015) Decontamination of wastewaters containing synthetic
671 organic dyes by electrochemical methods. An updated review. Appl Catal B Environ 166–
672 167:603–643. doi: 10.1016/j.apcatb.2014.11.016
673 Brillas E, Sauleda R, Casado J (1997) Peroxi-coagulation of aniline in acidic medium using an
674 oxygen diffusion cathode. J Electrochem Soc 144:2374. doi: 10.1149/1.1837821

675 Brillas E, Sirés I, Oturan MA (2009) Electro-Fenton process and related electrochemical
676 technologies based on Fenton's reaction chemistry. Chem Rev 109:6570–6631. doi:
677 10.1007/s00894-008-0358-0
678 Brito CDN, de Araújo DM, Martínez-Huitle CA, Rodrigo MA (2015) Understanding active
679 chlorine species production using boron doped diamond films with lower and higher
680 sp^3/sp^2 ratio. Electrochem commun 55:34–38. doi: 10.1016/j.elecom.2015.03.013
681 Catanho M, Malpass GRP, Motheo AJ (2006) Photoelectrochemical treatment of the dye
682 reactive red 198 using DSA® electrodes. Appl Catal B Environ 62:193–200. doi:
683 10.1016/j.apcatb.2005.07.011
684 Chaplin BP (2014) Critical review of electrochemical advanced oxidation processes for water
685 treatment applications. Environ Sci Process Impacts 16:1182–203. doi:
686 10.1039/c3em00679d
687 Cizmas L, Sharma VK, Gray CM, McDonald TJ (2015) Pharmaceuticals and personal care
688 products in waters: occurrence, toxicity, and risk. Environ Chem Lett 13:381–394. doi:
689 10.1007/s10311-015-0524-4
690 Comninellis C, Chen G (eds) (2010) Electrochemistry for the environment. Springer Nature,
691 pp 563. doi:10.1007/978-0-387-68318-8
692 Daskalaki VM, Fulgione I, Frontistis Z, et al (2013) Solar light-induced photoelectrocatalytic
693 degradation of bisphenol-A on TiO_2/ITO film anode and BDD cathode. Catal Today
694 209:74–78. doi: 10.1016/j.cattod.2012.07.026
695 Ding X, Ai Z, Zhang L (2012) Design of a visible light driven photo-electrochemical/electro-
696 Fenton coupling oxidation system for wastewater treatment. J Hazard Mater 239–
697 240:233–40. doi: 10.1016/j.jhazmat.2012.08.070
698 Ding X, Ai Z, Zhang L (2014) A dual-cell wastewater treatment system with combining anodic
699 visible light driven photoelectro-catalytic oxidation and cathodic electro-Fenton oxidation.
700 Sep Purif Technol 125:103–110. doi: 10.1016/j.seppur.2014.01.046
701 Dorfman LM, Adams GE (1973) Reactivity of the hydroxyl radical in aqueous solutions. 59
702 pp. Accession Number : ADD095248
703 dos Santos EV, Sáez C, Cañizares P, et al (2017) Treatment of ex-situ soil-washing fluids
704 polluted with petroleum by anodic oxidation , photolysis , sonolysis and combined
705 approaches. Chem Eng J 310:581–588. doi: 10.1016/j.cej.2016.05.015
706 dos Santos EV, Saez C, Martinez-Huitle CA, et al (2015) Combined soil washing and CDEO
707 for the removal of atrazine from soils. J Hazard Mater 300:129–134. doi:

10.1016/j.jhazmat.2015.06.064

dos Santos EV, Scialdone O (2018) Photo-electrochemical technologies for removing organic compounds in wastewater, Electrochemical water and wastewater treatment. Elsevier, pp. 239-266. doi:10.1016/B978-0-12-813160-2.00010-9.

El-Ghenymy A, Cabot PL, Centellas F, et al (2013) Mineralization of sulfanilamide by electro-Fenton and solar photoelectro-Fenton in a pre-pilot plant with a Pt/air-diffusion cell. Chemosphere 91:1324–31. doi: 10.1016/j.chemosphere.2013.03.005

El-Ghenymy A, Garcia-Segura S, Rodríguez RM, et al (2012) Optimization of the electro-Fenton and solar photoelectro-Fenton treatments of sulfanilic acid solutions using a pre-pilot flow plant by response surface methodology. J Hazard Mater 221–222:288–97. doi: 10.1016/j.jhazmat.2012.04.053

Esquivel K, Arriaga LG, Rodríguez FJ, et al (2009) Development of a TiO2 modified optical fiber electrode and its incorporation into a photoelectrochemical reactor for wastewater treatment. Water Res 43:3593–3603. doi: 10.1016/j.watres.2009.05.035

Fagan R, McCormack DE, Dionysiou DD, Pillai SC (2016) A review of solar and visible light active TiO2 photocatalysis for treating bacteria, cyanotoxins and contaminants of emerging concern. Mater Sci Semicond Process 42:2–14. doi: 10.1016/j.mssp.2015.07.052

Fang T, Yang C, Liao L (2012) Photoelectrocatalytic degradation of high COD dipterex pesticide by using TiO_2/Ni photo electrode. J Environ Sci (China) 24:1149–1156. doi: 10.1016/S1001-0742(11)60882-6

Faust BC, Hoigné J (1990) Photolysis of Fe (III)-hydroxy complexes as sources of OH radicals in clouds, fog and rain. Atmos Environ Part A, Gen Top 24:79–89. doi: 10.1016/0960-1686(90)90443-Q

Feng L, van Hullebusch ED, Rodrigo MA, et al (2013) Removal of residual anti-inflammatory and analgesic pharmaceuticals from aqueous systems by electrochemical advanced oxidation processes. A review. Chem Eng J 228:944–964

Fujishima A, Rao TN, Tryk DA (2000) Titanium dioxide photocatalysis. J Photochem Photobiol C Photochem Rev 1:1–21. doi: 10.1016/S1389-5567(00)00002-2

Ganiyu SO, Oturan N, Raffy S, et al (2016) Sub-stoichiometric titanium oxide (Ti_4O_7) as a suitable ceramic anode for electrooxidation of organic pollutants: A case study of kinetics, mineralization and toxicity assessment of amoxicillin. Water Res 106:171–182. doi: 10.1016/j.watres.2016.09.056

741 Ganiyu SO, Oturan N, Raffy S, et al (2017) Use of sub-stoichiometric titanium oxide as a
742 ceramic electrode in anodic oxidation and electro-Fenton degradation of the beta-blocker
743 propranolol: Degradation kinetics and mineralization pathway. Electrochim Acta
744 242:344–354. doi: 10.1016/j.electacta.2017.05.047
745 Ganiyu SO, Zhou M, Martínez-huitle CA (2018) Heterogeneous electro-Fenton and
746 photoelectro-Fenton processes : A critical review of fundamental principles and
747 application for water/wastewater treatment. Appl Catal B Environ 235:103–129. doi:
748 10.1016/j.apcatb.2018.04.044
749 Ganzenko O, Oturan N, Sirés I, et al (2018) Fast and complete removal of the 5-fluorouracil
750 drug from water by electro-Fenton oxidation. Environ Chem Lett 16:281–286. doi:
751 10.1007/s10311-017-0659-6
752 Garcia-Rodriguez O, Lee YY, Olvera-Vargas H, et al (2018) Mineralization of electronic
753 wastewater by electro-Fenton with an enhanced graphene-based gas diffusion cathode.
754 Electrochim Acta 276:12–20. doi: 10.1016/j.electacta.2018.04.076
755 Garcia-Segura S, Brillas E (2014) Advances in solar photoelectro-Fenton: Decolorization and
756 mineralization of the Direct Yellow 4 diazo dye using an autonomous solar pre-pilot plant.
757 Electrochim Acta 140:384–395. doi: 10.1016/j.electacta.2014.04.009
758 Garcia-Segura S, Cavalcanti EB, Brillas E (2014) Mineralization of the antibiotic
759 chloramphenicol by solar photoelectro-Fenton. From stirred tank reactor to solar pre-pilot
760 plant. Appl Catal B Environ 144:588–598. doi: 10.1016/j.apcatb.2013.07.071
761 Garcia-Segura S, Dosta S, Guilemany JM, Brillas E (2013) Solar photoelectrocatalytic
762 degradation of Acid Orange 7 azo dye using a highly stable TiO_2 photoanode synthesized
763 by atmospheric plasma spray. Appl Catal B Environ 132–133:142–150. doi:
764 10.1016/j.apcatb.2012.11.037
765 Garza-Campos B, Brillas E, Hernandez-Ramirez A, et al (2016) Salicylic acid degradation by
766 advanced oxidation processes. Coupling of solar photoelectro-Fenton and solar
767 heterogeneous photocatalysis. J Hazard Mater 319:34–42. doi:
768 10.1016/j.jhazmat.2016.02.050
769 Garza-Campos BR, Guzmán-Mar JL, Reyes LH, et al (2014) Coupling of solar photoelectro-
770 Fenton with a BDD anode and solar heterogeneous photocatalysis for the mineralization
771 of the herbicide atrazine. Chemosphere 97:26–33. doi:
772 10.1016/j.chemosphere.2013.10.044
773 Glaze WH, Kang JW, Chapin DH (1987) The chemistry of water-treatment processes involving

ozone, hydrogen-peroxide and ultraviolet-radiation. Ozone Sci Eng 9:335–352.

Gligorovski S, Strekowski R, Barbati S, Vione D (2015) Environmental implications of hydroxyl radicals (•OH). Chem Rev 115:13051–13092. doi: 10.1021/cr500310b

Goldstein S, Aschengrau D, Diamant Y, Rabani J (2007) Photolysis of aqueous H_2O_2: Quantum yield and applications for polychromatic UV actinometry in photoreactors. Environ Sci Technol 41:7486–7490. doi: 10.1021/es071379t

Khataee AR, Safarpour M, Zarei M, Aber S (2012) Combined heterogeneous and homogeneous photodegradation of a dye using immobilized TiO_2 nanophotocatalyst and modified graphite electrode with carbon nanotubes. J Mol Catal A Chem 363–364:58–68. doi: 10.1016/j.molcata.2012.05.016

Lahkimi A, Oturan MA, Oturan N, Chaouch M (2007) Removal of textile dyes from water by the electro-Fenton process. Environ Chem Lett 5:35–39. doi: 10.1007/s10311-006-0058-x

Lazar M, Varghese S, Nair S (2012) Photocatalytic water treatment by titanium dioxide: Recent updates. Catalysts 2:572–601. doi: 10.3390/catal2040572

Le TXH, Bechelany M, Lacour S, et al (2015a) High removal efficiency of dye pollutants by electron-Fenton process using a graphene based cathode. Carbon N Y 94:1003–1011. doi: 10.1016/j.carbon.2015.07.086

Le TXH, Bechelany M, Champavert J, Cretin M (2015b) A highly active based graphene cathode for electro-Fenton reaction. RSC Adv 5:42536–42539. doi:10.1039/C5RA04811G

Le TXH, Charmette C, Bechelany M, Cretin M (2016) Facile preparation of porous carbon cathode to eliminate paracetamol in aqueous medium using electro-Fenton system. Electrochim Acta 188:378–384. doi: 10.1016/j.electacta.2015.12.005

Liu X, Zhang H, Liu C, et al (2014) UV and visible light photoelectrocatalytic bactericidal performance of 100% {1 1 1} faceted rutile TiO_2 photoanode. Catal Today 224:77–82. doi: 10.1016/j.cattod.2013.09.041

Liu Y, Li J, Zhou B, et al (2009) Comparison of photoelectrochemical properties of TiO_2-nanotube-array photoanode prepared by anodization in different electrolyte. Environ Chem Lett 7:363–368. doi: 10.1007/s10311-008-0180-z

Luo H, Li C, Wu C, et al (2015) Electrochemical degradation of phenol by in situ electro-generated and electro-activated hydrogen peroxide using an improved gas diffusion cathode. Electrochim Acta 186:486–493. doi: 10.1016/j.electacta.2015.10.194

807 Luo Y, Guo W, Ngo HH, et al (2014) A review on the occurrence of micropollutants in the
808 aquatic environment and their fate and removal during wastewater treatment. Sci Total
809 Environ 473–474:619–41. doi: 10.1016/j.scitotenv.2013.12.065
810 Malato S, Fernandez-Ibanez P, Maldonado MI, et al (2009) Decontamination and disinfection
811 of water by solar photocatalysis: Recent overview and trends. Catal Today 147:1–59. doi:
812 10.1016/j.cattod.2009.06.018
813 Martínez-Huitle CA, Brillas E (2009) Decontamination of wastewaters containing synthetic
814 organic dyes by electrochemical methods: A general review. Appl. Catal. B Environ.
815 87:105–145.
816 Martínez-Huitle CA, Rodrigo MA, Sirés I, Scialdone O (2015) Single and coupled
817 electrochemical processes and reactors for the abatement of organic water pollutants: A
818 critical review. Chem Rev 115:13362–13407. doi: 10.1021/acs.chemrev.5b00361
819 Merényi G, Lind J, Naumov S, Sonntag C von (2010) Reaction of ozone with hydrogen
820 peroxide (peroxone process): A revision of current mechanistic concepts based on
821 thermokinetic and quantum-chemical considerations. Environ Sci Technol 44:3505–7.
822 doi: 10.1021/es100277d
823 Moreira FC, Boaventura RAR, Brillas E, Vilar VJP (2017) Electrochemical advanced oxidation
824 processes: A review on their application to synthetic and real wastewaters. Appl Catal B
825 Environ 202:217–261. doi: 10.1016/j.apcatb.2016.08.037
826 Mousset E, Frunzo L, Esposito G, et al (2016a) A complete phenol oxidation pathway obtained
827 during electro-Fenton treatment and validated by a kinetic model study. Appl Catal B
828 Environ 180:189–198.
829 Mousset E, Huang Weiqi V, Foong Yang Kai B, et al (2017a) A new 3D-printed
830 photoelectrocatalytic reactor combining the benefits of a transparent electrode and the
831 Fenton reaction for advanced wastewater treatment. J Mater Chem A 5:24951–24964. doi:
832 10.1039/C7TA08182K
833 Mousset E, Huguenot D, Van Hullebusch ED, et al (2016b) Impact of electrochemical treatment
834 of soil washing solution on PAH degradation efficiency and soil respirometry. Environ
835 Pollut 211:354–362. doi: 10.1016/j.envpol.2016.01.021
836 Mousset E, Ko ZT, Syafiq M, et al (2016c) Electrocatalytic activity enhancement of a graphene
837 ink-coated carbon cloth cathode for oxidative treatment. Electrochim Acta 222:1628–
838 1641. doi: 10.1016/j.electacta.2016.11.151
839 Mousset E, Oturan N, Oturan MA (2018a) An unprecedented route of OH radical reactivity

evidenced by an electrocatalytical process: Ipso-substitution with perhalogenocarbon compounds. Appl Catal B Environ 226:135–146. doi: 10.1016/j.apcatb.2017.12.028

Mousset E, Oturan N, van Hullebusch ED, et al (2013) A new micelle-based method to quantify the Tween 80® surfactant for soil remediation. Agron Sustain Dev 33:839–846. doi: 10.1007/s13593-013-0140-2

Mousset E, Oturan N, van Hullebusch ED, et al (2014a) Influence of solubilizing agents (cyclodextrin or surfactant) on phenanthrene degradation by electro-Fenton process - Study of soil washing recycling possibilities and environmental impact. Water Res 48:306–316. doi: 10.1016/j.watres.2013.09.044

Mousset E, Oturan N, van Hullebusch ED, et al (2014b) Treatment of synthetic soil washing solutions containing phenanthrene and cyclodextrin by electro-oxidation. Influence of anode materials on toxicity removal and biodegradability enhancement. Appl Catal B Environ 160–161:666–675. doi: 10.1016/j.apcatb.2014.06.018

Mousset E, Pechaud Y, Oturan N, Oturan MA (2019a) Charge transfer/mass transport competition in advanced hybrid electrocatalytic wastewater treatment: Development of a new current efficiency relation. Appl Catal B Environ 240:102–111. doi: 10.1016/j.apcatb.2018.08.055

Mousset E, Pontvianne S, Pons M-N (2018b) Fate of inorganic nitrogen species under homogeneous Fenton combined with electro-oxidation/reduction treatments in synthetic solutions and reclaimed municipal wastewater. Chemosphere 201:6–12. doi: 10.1016/j.chemosphere.2018.02.142

Mousset E, Puce M, Pons M-N (2019b) Advanced electro-oxidation with boron-doped diamond for acetaminophen removal from real wastewater in a microfluidic reactor – Kinetics and mass transfer studies. ChemElectroChem 6:2908–2916. doi: 10.1002/celc.201900182

Mousset E, Quackenbush L, Schondek C, et al (2020) Effect of homogeneous Fenton combined with electron transfer on the fate of inorganic chlorinated species in synthetic and reclaimed municipal wastewater. Electrochim Acta. doi: 10.1016/j.electacta.2019.135608

Mousset E, Wang Z, Hammaker J, Lefebvre O (2017b) Electrocatalytic phenol degradation by a novel nanostructured carbon fiber brush cathode coated with graphene ink. Electrochim Acta. doi: 10.1016/j.electacta.2017.11.104

Mousset E, Wang Z, Hammaker J, Lefebvre O (2016d) Physico-chemical properties of pristine graphene and its performance as electrode material for electro-Fenton treatment of wastewater. Electrochim Acta 214:217–230. doi: 10.1016/j.electacta.2016.08.002

873 Mousset E, Wang Z, Lefebvre O (2016e) Electro-Fenton for control and removal of
874 micropollutants - Process optimization and energy efficiency. Water Sci Technol
875 74:2068–2074. doi:10.2166/wst.2016.353
876 Mousset E, Zhou M (2017) Graphene-based nanostructured materials for advanced
877 electrochemical water/wastewater treatment. In: Thomas S, Thankappan A (eds)
878 Polymeric and nanostructured materials: Synthesis, properties and advanced applications,
879 Apple Acad. pp. 321–358. ISBN:9781771886444
880 Nidheesh PV. (2018) Removal of organic pollutants by peroxicoagulation. Environ Chem Lett
881 16:1283–1292. doi: 10.1007/s10311-018-0752-5
882 Oturan MA, Aaron J-J (2014) Advanced oxidation processes in water/wastewater treatment:
883 Principles and applications. A Review. Crit Rev Environ Sci Technol 44:2577–2641. doi:
884 10.1080/10643389.2013.829765
885 Oturan N, Brillas E, Oturan MA (2012) Unprecedented total mineralization of atrazine and
886 cyanuric acid by anodic oxidation and electro-Fenton with a boron-doped diamond anode.
887 Environ Chem Lett 10:165–170. doi: 10.1007/s10311-011-0337-z
888 Panizza M, Cerisola G (2009) Direct and mediated anodic oxidation of organic pollutants.
889 Chem Rev 109:6541–6569. doi: 10.1021/cr9001319
890 Panizza M, Martinez-Huitle CA (2013) Role of electrode materials for the anodic oxidation of
891 a real landfill leachate--comparison between Ti-Ru-Sn ternary oxide, PbO_2 and boron-
892 doped diamond anode. Chemosphere 90:1455–60. doi:
893 10.1016/j.chemosphere.2012.09.006
894 Pelaez M, Nolan NT, Pillai SC, et al (2012) A review on the visible light active titanium dioxide
895 photocatalysts for environmental applications. Appl Catal B Environ 125:331–349. doi:
896 10.1016/j.apcatb.2012.05.036
897 Ramirez RJ, Pineda CA, Álvarez AA, et al (2015) H_2O_2-assisted TiO_2 generation during the
898 photoelectrocatalytic process to decompose the acid green textile dye by Fenton reaction.
899 J Photochem Photobiol A Chem 305:51–59. doi: 10.1016/j.jphotochem.2015.03.004
900 Ren G, Zhou M, Su P, et al (2018) Highly energy-efficient removal of acrylonitrile by peroxi–
901 coagulation with modified graphite felt cathode: influence factors, possible mechanism.
902 Chem Eng J 343:467–476. doi:10.1016/j.cej.2018.02.115
903 Schneider J, Matsuoka M, Takeuchi M, et al (2014) Understanding TiO_2 photocatalysis:
904 Mechanisms and materials. Chem Rev 114:9919–9986. doi: 10.1021/cr5001892
905 Scialdone O, Guarisco C, Galia A, et al (2010) Anodic abatement of organic pollutants in water

906 in micro reactors. J Electroanal Chem 638:293–296. doi: 10.1016/j.jelechem.2009.10.031
907 Shi H, Ni J, Zheng T, et al (2020) Remediation of wastewater contaminated by antibiotics. A
908 review. Environ Chem Lett 18:345–360. doi: 10.1007/s10311-019-00945-2
909 Shukla S, Oturan MA (2015) Dye removal using electrochemistry and semiconductor oxide
910 nanotubes. Environ Chem Lett 13:157–172. doi: 10.1007/s10311-015-0501-y
911 Sirés I, Brillas E, Oturan MA, et al (2014) Electrochemical advanced oxidation processes:
912 Today and tomorrow. A review. Environ Sci Pollut Res 21:8336–8367. doi:
913 10.1007/s11356-014-2783-1
914 Sirés I, Garrido JA, Rodríguez RM, et al (2007) Catalytic behavior of the Fe^{3+}/Fe^{2+} system in
915 the electro-Fenton degradation of the antimicrobial chlorophene. Appl Catal B Environ
916 72:382–394. doi: 10.1016/j.apcatb.2006.11.016
917 Sopaj F (2013) Study of the influence of electrode material in the application of electrochemical
918 advanced oxidation processes to removal of pharmaceutical pollutants from water.
919 University of Paris-Est. https://tel.archives-ouvertes.fr/tel-00985537
920 Stefan MI (ed) (2017) Advanced oxidation processes for water treatment: fundamentals and
921 applications. IWA Publishing, London, UK. ISBN13:9781780407180
922 Sun Y, Pignatello JJ (1993) Photochemical reactions involved in the total mineralization of 2,4-
923 D by iron(3+)/hydrogen peroxide/UV. Environ Sci Technol 27:304–310. doi:
924 10.1021/es00039a010
925 UNESCO (2017) Wastewater, The Untapped Resource. United Nations World Water
926 Development Report. (http://www.unesco.org/new/en/natural-
927 sciences/environment/water/wwap/wwdr/2017-wastewater-the-untapped-resource/)
928 Vasudevan S, Oturan MA (2014) Electrochemistry: As cause and cure in water pollution-an
929 overview. Environ Chem Lett 12:97–108. doi: 10.1007/s10311-013-0434-2
930 Von Sonntag C (2008) Advanced oxidation processes: Mechanistic aspects. Water Sci Technol
931 58:1015–1021. doi: 10.2166/wst.2008.467
932 Xie YB, Li XZ (2006) Interactive oxidation of photoelectrocatalysis and electro-Fenton for azo
933 dye degradation using TiO_2–Ti mesh and reticulated vitreous carbon electrodes. Mater
934 Chem Phys 95:39–50. doi: 10.1016/j.matchemphys.2005.05.048
935 Xu Z, Li X, Li J, et al (2013) Effect of CoOOH loading on the photoelectrocatalytic
936 performance of WO_3 nanorod array film. Appl Surf Sci 284:285–290. doi:
937 10.1016/j.apsusc.2013.07.095
938 Yu F, Zhou M, Yu X (2015) Cost-effective electro-Fenton using modified graphite felt that

dramatically enhanced on H_2O_2 electro-generation without external aeration. Electrochim Acta 163:182–189. doi: 10.1016/j.electacta.2015.02.166

Zhai C, Zhu M, Ren F, et al (2013) Enhanced photoelectrocatalytic performance of titanium dioxide/carbon cloth based photoelectrodes by graphene modification under visible-light irradiation. J Hazard Mater 263 Pt 2:291–8. doi: 10.1016/j.jhazmat.2013.09.013

Zhao X, Liu H, Qu J (2010) Photoelectrocatalytic degradation of organic contaminant at hybrid BDD-$ZnWO_4$ electrode. Catal Commun 12:76–79. doi: 10.1016/j.catcom.2010.08.013

Zhao X, Qu J, Liu H, et al (2009) Photoelectrochemical degradation of anti-inflammatory pharmaceuticals at Bi_2MoO_6-boron-doped diamond hybrid electrode under visible light irradiation. Appl Catal B Environ 91:539–545. doi: 10.1016/j.apcatb.2009.06.025

Zhou B, Zhao X, Liu H, et al (2010) Visible-light sensitive cobalt-doped $BiVO_4$ (Co-$BiVO_4$) photocatalytic composites for the degradation of methylene blue dye in dilute aqueous solutions. Appl Catal B Environ 99:214–221. doi: 10.1016/j.apcatb.2010.06.022

Zhou L, Zhou M, Hu Z, et al (2014) Chemically modified graphite felt as an efficient cathode in electro-Fenton for p-nitrophenol degradation. Electrochim Acta 140:376–383. doi: 10.1016/j.electacta.2014.04.090